CMS Physics Analysis Summary

Contact: cms-pag-conveners-higgs@cern.ch 2013/05/15

Search for $t\bar{t}H$ production in events with $H \to \gamma\gamma$ at $\sqrt{s} = 8\,\text{TeV}$ collisions

The CMS Collaboration

Abstract

We present the results of the search for the associated production of the Higgs boson with a $t\bar{t}$ pair, using for the first time the events where the Higgs boson decays to two photons. To maximize acceptance and sensitivity to such a small signal, we device two different sets of event selection criteria, optimized for leptonic and hadronic $t\bar{t}$ decays. We analyze $19.6\,\text{fb}^{-1}$ of 8 TeV pp collisions and found no significant excess over the background-only predictions. We thus proceed to set an observed (expected) 95% confidence level upper limit on the $t\bar{t}H$ production cross section times $BR(H \to \gamma\gamma)$ of 5.4 (5.3) times the standard model value, corresponding to 1.6 fb, for a Higgs boson of $m_H = 125\,\text{GeV}$.

1 Introduction

Just after the discovery of a new particle by CMS and ATLAS [1, 2] its mass is already known with good precision. The analyses carried out so far seem to confirm that this particle is compatible with a standard model (SM) Higgs boson with mass around 125 GeV. The upcoming challenge for the experiments is now to measure the coupling of the new boson to the existing SM particles. It is of great interest, in particular, to measure the coupling to the top quark as, due to its large mass, it plays a special role in the context of electroweak symmetry breaking. In order to directly probe the $\mathrm{t\bar{t}H}$ interaction vertex, a very rare production mechanism has to be searched for, in which the Higgs boson is produced in association with a top quark-antiquark pair. This process is expected to have a very small cross section in 8 TeV pp collisions, amounting to only 130 fb at next-to-leading order (NLO) [3].

Observing this process represents the only opportunity to directly probe the $\mathrm{t\bar{t}H}$ vertex. Direct Higgs boson production, which proceeds through a quark loop dominated by the top quark contribution, also allows measuring the coupling between the top quark and Higgs boson, but only under the assumption that there are no contributions beyond the SM to the loop. The top Yukawa coupling can be directly measured by performing the ratio to other production modes, in channels with the same Higgs boson decay mode. The current precision on the top mass measurement of $\sim 0.5\%$ [4, 5] translates into a Yukawa coupling between the top quark and the Higgs field equal to one within an uncertainty of about five per thousand. This closeness to a natural value (i.e. one) led to speculations about a possible special role of the top quark in the electroweak symmetry breaking mechanism. Several new physics scenarios [6–9] predict the existence of unobserved heavy particles, such as top quark partners, that would decay into a top quark and a Higgs boson. The observation of a significant deviation of the measured rate of $\mathrm{t\bar{t}H}$ production with respect to SM predictions would thus be an indirect indication of unknown phenomena. The first searches for $\mathrm{t\bar{t}H}$ production have been performed at the CDF and D0 experiments by looking at the $b\bar{b}$ decays of the Higgs boson, setting 95% confidence level (CL) upper limits on the $\mathrm{t\bar{t}H}$ production cross section times $BR(H \to b\bar{b})$ above 10 times the standard model predictions [10, 11]. Searches for $\mathrm{t\bar{t}H}$ in the same decay mode have been performed also by ATLAS and CMS using $5\,\mathrm{fb}^{-1}$ of 7 TeV (and 8 TeV for CMS) pp collisions [12, 13] with enhanced sensitivity. The currently most sensitive search is the CMS one that sets an upper limit of 5.8 times $\sigma_{\mathrm{t\bar{t}H}} BR(H \to b\bar{b})$. No results are available in other Higgs boson decay modes.

We investigate for the first time the production of $\mathrm{t\bar{t}H}$ in events where the Higgs boson decays to photons. A Feynman diagram for the process of associated top quarks and Higgs boson production is shown in Fig. 1, together with each top quark decaying to a W boson and a b quark, and the Higgs boson decaying to photons.

This final state allows to reconstruct the Higgs boson invariant mass with excellent resolution. The channel is limited from the extremely low branching ratio of Higgs boson decaying into two photons, i.e. $BR(H \to \gamma\gamma) = 0.0023$ at $m_H = 125\,\mathrm{GeV}$ [14]. In fact, the product of the $\mathrm{t\bar{t}H}$ production cross section and $BR(H \to \gamma\gamma)$ amounts to 0.3 fb at NLO, leading to only a handful of events in the full 2012 dataset. To maximize signal efficiency, we devise event selections that collect both hadronic $\mathrm{t\bar{t}} \to \mathrm{bq\bar{q}'\bar{b}q\bar{q}'}$ and leptonic $\mathrm{t\bar{t}} \to \mathrm{b\ell\nu\bar{b}q\bar{q}'}$, $\mathrm{t\bar{t}} \to \mathrm{b\ell\nu\bar{b}\ell\nu}$, decays, where ℓ denotes either an electron or a muon.

2 Experimental Setup

This measurement uses data from proton-proton collisions, produced at a center-of-mass energy of 8 TeV, corresponding to an integrated luminosity of $19.6 \pm 0.9\,\mathrm{fb}^{-1}$ [15]. The data were

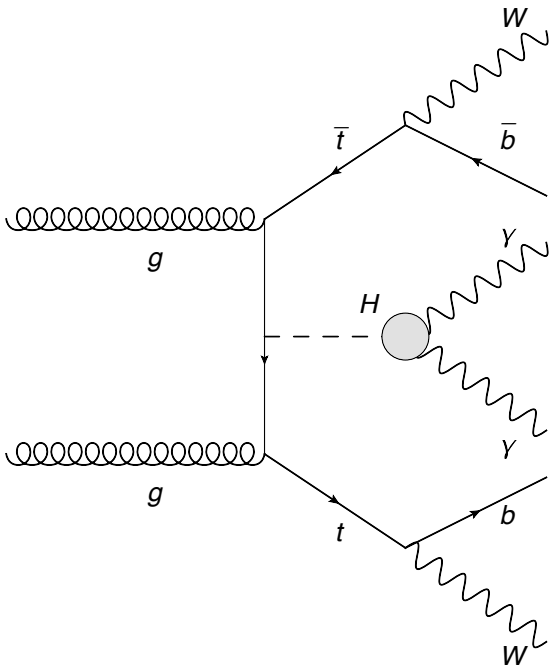

Figure 1: Feynman diagram for one of the LO diagrams of $t\bar{t}H$ production at pp colliders, with Higgs boson decaying to photons. The shaded area represents the fermionic and bosonic loop connecting the Higgs boson to photons.

collected by the CMS detector at the Large Hadron Collider (LHC) in 2012. The data has been recorded through the High Level Trigger (HLT) paths which rely on the presence in the event of two photons with large momentum transverse to the beam axis, p_T, similarly to Ref.[16].

A detailed description of the CMS detector can be found elsewhere [17]. Its central feature is a 3.8 T superconducting solenoid of 6 m internal diameter. Within its field volume are the silicon tracker, the crystal electromagnetic calorimeter (ECAL), and the brass/scintillator sampling hadron calorimeter (HCAL). The muon system, composed of drift tubes, cathode strip chambers, and resistive-plate chambers, is installed outside the solenoid, embedded in the steel return yoke. CMS uses a right-handed coordinate system, with the origin at the nominal interaction point, the x axis pointing to the center of the LHC, the y axis pointing up (perpendicular to the LHC plane), and the z axis along the counterclockwise-beam direction. The polar angle θ is measured from the positive z axis and the azimuthal angle ϕ is measured in the x-y plane. The pseudorapidity η is defined as $-\ln[\tan(\theta/2)]$.

Photon candidates are reconstructed from the energy deposits in the ECAL, grouping its channels into a supercluster. The superclustering algorithms achieve an almost complete collection of the energy of photons (and electrons) that convert into electron-positron pairs (emit bremstrahlung) in the material in front of the ECAL. In the barrel region, superclusters are formed from five-crystal-wide strips in η, centred on the locally most energetic crystal (seed), and have a variable extension in ϕ. In the endcaps, where the crystals are arranged according to an x-y rather than an η-ϕ geometry, matrices of 5×5 crystals (which may partially overlap) around the most energetic crystals are merged if they lie within a narrow ϕ road. The photon candidates are collected within the ECAL fiducial region $|\eta| < 2.5$, excluding the barrel-endcap transition region $1.4442 < |\eta| < 1.566$. Isolation requirements are applied to photon candidates by looking at neighbouring particle candidates reconstructed with the particle-flow (PF) event reconstruction technique [18]. Details on photon reconstruction and identification are

found in [16].

Jets are defined by clustering PF particle candidates with the anti-k_T algorithm [19] with a distance parameter of 0.5. The jet energy resolution is typically 15% at 10 GeV and 8% at 100 GeV. The jet energy resolution in simulated jets is known to deviate from what is observed in data, thus additional corrections are applied. Jets are required to be inside the tracker acceptance ($|\eta| < 2.4$), to increase the reconstruction efficiency and the precision of the energy measurement using PF techniques. Jet energy corrections are applied to account for the non-linear response of the calorimeters to the particle energies and other instrumental effects. These corrections are based on in situ measurements using dijet and γ + jet data samples [20]. Pileup activity has an effect on jet reconstruction by contributing additional particles to the reconstructed jets. The average energy density due to pileup is evaluated in each event and the corresponding energy is subtracted from each jet [21]. A jet identification requirement, primarily based on the energy balance between charged and neutral hadrons in a jet, is applied to remove misidentified jets. Jets are required to have $p_T > 25$ GeV.

To identify jets originating from the hadronization of bottom quarks, the Combined Secondary Vertex (CSV) b-tagging algorithm [22] is employed. The algorithm identifies jets from b-hadron decays by identifying their displaced decay vertex. Throughout this analysis we use the medium working point of this tagger, which provides an efficiency for b jets of about 70% and a misidentification probability for jets from light quarks and gluons of about 1%. The efficiency of b-tagging in Monte Carlo jets is corrected for known discrepancy between data and Monte Carlo.

Muons are measured [23] with the combination of the tracker and the muon system, in the pseudorapidity range $|\eta| < 2.4$. Electrons are detected [24] as tracks in the tracker pointing to energy clusters in the ECAL up to $|\eta| = 2.5$. Both muons and electrons are required to have p_T greater than 20 GeV. Isolation requirements are enforced on electrons and muons with similar techniques as used in the case of photons. Additional corrections are applied to correct for known discrepancy between data and simulation. The full details of the electron and muon identification criteria are described elsewhere [25].

3 Analysis Strategy and Simulation

The analysis strategy is to devise an event selection that reflects the multibody $t\bar{t}H$ final state, and fit the diphoton mass distribution, where the diphoton spectrum sidebands will be used to fit the distribution of the backgrounds. The presence of a signal around 125 GeV characterized by a sharp peak compatible with detector resolutions is allowed. The expected diphoton mass distribution for the signal and the composition of the signal in terms of several Higgs boson production processes, is taken from studies of the simulation.

Various Higgs boson production process simulated samples are used for this analysis. Events in which the Higgs boson is produced in association with a top quark-antiquark pair are simulated at diagram level with the LO matrix element generator PYTHIA 6.4 [26]. Of the other production modes, gluon fusion ($gg \to H$) and vector boson fusion ($qq \to qqH$) are simulated with the POWHEG BOX [27–29] at NLO, and interfaced to PYTHIA for parton showering and hadronization, whereas production associated with weak bosons ($qq \to WH/ZH$) is simulated at LO with PYTHIA, similarly to $t\bar{t}H$ production. The signal is simulated for mass values with steps of 5 GeV between 100 and 150 GeV, with a finner binning of 1-2 GeV in the region close to the observed mass. The modeling of the underlying event is done through the Z2* tune of PYTHIA [30]. All of these simulated samples make use of a GEANT4-based [31] simulation of the response of the CMS detector. The profile of the number of reconstructed vertices of

simulated events has been corrected to match the actual distribution in data.

The main backgrounds are the production of top quarks and either real or fake photons in the final state, and the production of high p_T photons in association with many jets, including heavy flavor jets.

A control sample is defined in the data to perform studies of the expected background. This is done by analyzing events which have been recorded with single photon HLT paths, and inverting the photon identification requirements on one of the two photons used to reconstruct the Higgs boson signal. To take into account the fact that the efficiency of photon isolation is not constant as a function of transverse momentum and pseudorapidity, a two-dimensional reweighting procedure is applied on the leading and subleading photon candidates of such events. The reweighting is performed so as to match the photon transverse momentum and pseudorapidity spectra to the ones of photons populating the signal region. In this way we obtain a control sample with similar kinematic properties as the data, yet selecting completely independent samples from a statistical point of view.

The choice of the background parametrisation is a key component for the signal extraction, since the background is obtained by fitting the observed diphoton mass distributions in each event category (hadronic or leptonic) over the range $100 < m_{\gamma\gamma} < 180$ GeV. This choice is based upon a data-driven criterion, which starts by finding possible "truth" models, which are the functions able to give a good fit of the observed mass distribution in the control sample. The final background model, for each event category, is chosen to be the one giving a maximum potential bias on the number of fitted background events in a diphoton mass region corresponding to 1 FWHM of the signal shape less than five times the statistical uncertainty on the background. This study is based on toy MCs generated from the possible truth models and fitted with different class of functions with an increasing number of degrees of freedom. The study aims at identifying the function with less degrees of freedom which fulfills these conditions, which guarantees that the systematic associated to the background shape can be safely neglected.

4 Event Selection

Two sets of event selection criteria are defined, which aim to search for hadronic

$$t\bar{t}H \to (t\bar{t} \to b\bar{b}q\bar{q}q\bar{q})(H \to \gamma\gamma)$$

and leptonic

$$t\bar{t}H \to (t\bar{t} \to b\bar{b}q\bar{q}\ell\bar{\nu})(H \to \gamma\gamma) \quad + \quad \text{h.c.}$$

top pair decays in $t\bar{t}H$ events. The event selections has been obtained starting from the study of a loose event selection, called preselection in the following. Event preselection is defined by requiring two photons with transverse momentum greater than, respectively, 33 and 25 GeV, so as to ensure high efficiency over the diphoton HLT paths, and two or more jets in the event for the hadronic channel preselection, plus an high p_T electron or muon for the leptonic channel. The distribution of some kinematic variables after preselection requirements are shown in Fig. 2: the jet multiplicity (top) and the b-jet multiplicity (bottom), defined with the medium working point of the CSV tagger. The left plots show the distribution in the preselection for the hadronic sample, while the right plots are for the leptonic sample. The plots compare the data from the signal region sidebands (black markers), defined as events with $115 < m_{\gamma\gamma} < 135$ and the data from the control sample (green histogram) to simulated $t\bar{t}H$ events(red line). All contributions are normalized to the integral of the signal region sidebands.

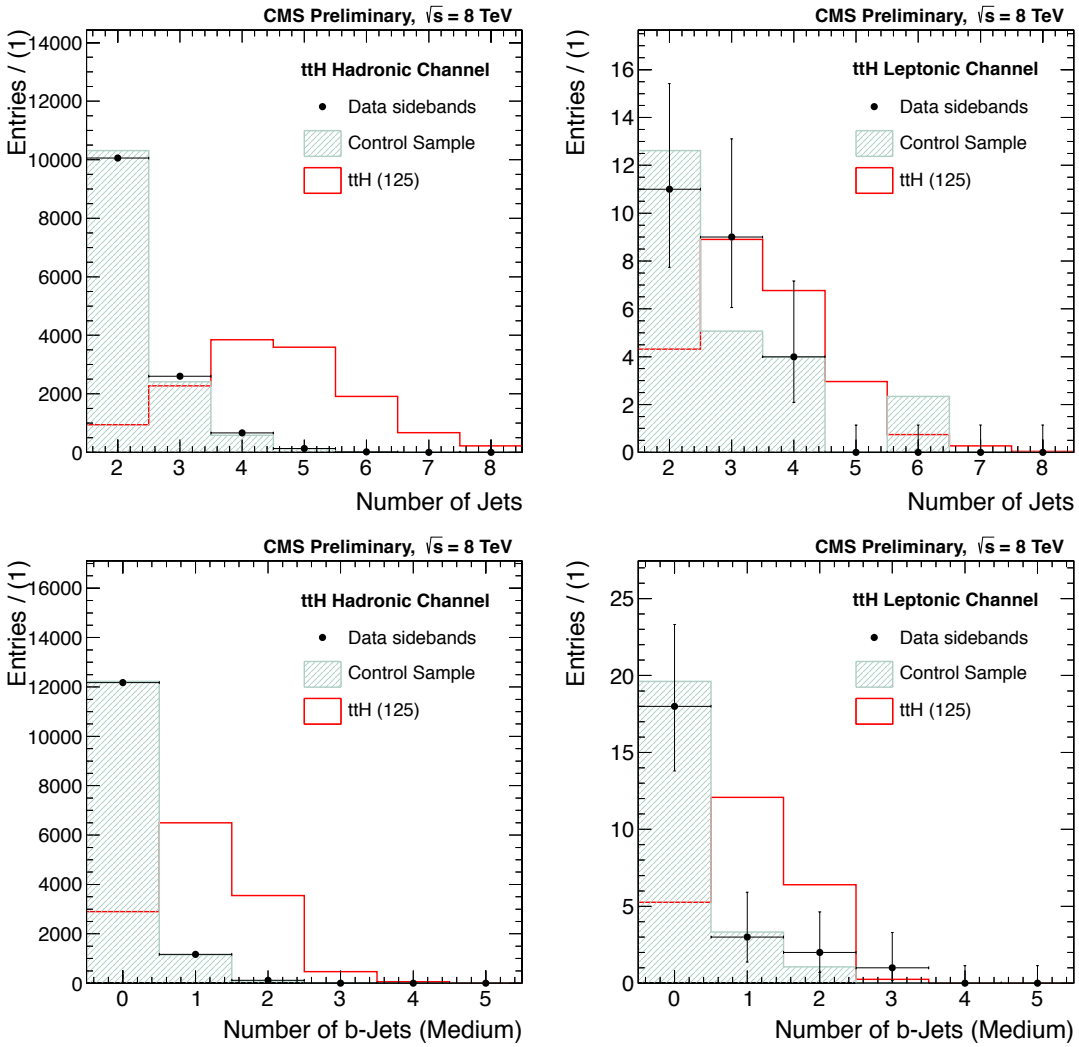

Figure 2: Distribution of some kinematic variables after preselection requirements: the jet multiplicity (top) and the b-jet multiplicity (bottom), defined with the medium working point of the CSV tagger. On the left are shown the plots for the hadronic selection, while on the right the leptonic selections is shown. The plots compare the data from the signal region sidebands (black markers) and the data from the control sample (green histogram) to simulated $t\bar{t}H$ (red line) events. All contributions are normalized to the integral of the signal region sidebands.

The two channels benefit from the same photon selection, which requires the leading photon to have a transverse momentum greater than 60 GeV $\cdot m_{\gamma\gamma}/120$ GeV, and the subleading photon to have $p_{\mathrm{T}} > 25$ GeV. The adoption of a variable threshold on the leading photon is aimed at increasing efficiency while minimize the trigger turn-on effects. In addition to this, both channels require the presence of at least one b-tagged jet. The hadronic channel is then defined by the requirement of at least four more jets in the event and no lepton, whereas the leptonic channel is defined by requiring at least one more jet in the event and at least one lepton (electron or muon).

The diphoton invariant mass spectra after full selections are shown in Fig. 3, on the left for the hadronic channel and on the right for the leptonic channel. The data are fitted with a simple exponential for the leptonic channel, and a second order polynomial for the hadronic channel.

Process	Hadronic Channel	Leptonic Channel
$t\bar{t}H$	0.567 (87%)	0.429 (97%)
$gg \to H$	0.059 (9%)	0 (0%)
VBF H	0.006 (1%)	0 (0%)
WH/ZH	0.019 (3%)	0.013 (3%)
Total signal	0.65	0.44

Table 1: Expected signal yields in 19.6 fb^{-1} of data after full event selections. Different production processes are shown. In parenthesis are given the relative fraction of the several Higgs boson production processes, normalized to the entire Higgs boson signal.

The result of the fit is shown on the plot, together with the uncertainty bands corresponding to 68% and 95% probability. The expected contribution of a SM Higgs boson is also shown as a blue histogram.

The expected signal event yields after selections for a standard model Higgs Boson with $m_H = 125$ GeV, split in its main production modes, are summarized in Tab. 1. As can be seen the contribution of production modes other than $t\bar{t}H$ is minor.

5 Systematic Uncertainties

All systematic uncertainties discussed in the following apply to the Higgs boson signal only. The theoretical systematic uncertainties considered on the production cross sections are calculated following the recommendation of the LHC Higgs Cross Section working group [3]. Systematics affecting the background are not considered as the bias study shows that they can be safely neglected. We thus consider the following sources of experimental systematic uncertainties:

Luminosity: The uncertainty on the luminosity measurement is 4.4% [15].

Photon reconstruction: The considered sources of systematic uncertainties for photon reconstruction are applied at single photon level and then propagated into the diphoton signal model using the MC. For the photon identification we use as systematic error the largest uncertainty in the fiducial region on the data to MC efficiency scale factor as measured using a tag-and-probe technique applied on $Z \to e^+e^-$ events (3.0% in EB, 4.0% in EE). For the uncertainties related to the photon scale and resolution we smear and shift the photon energy within the known uncertainty for both photons (the uncertainty is mostly due to the extrapolation of the systematic from electrons to photons, since it is studied with $Z \to e^+e^-$ and then applied to photons). This uncertainty reflects on both the shape and normalization of the Higgs boson diphoton signal.

Jet energy scale: This uncertainty is evaluated by modifying the jet transverse momenta by one standard deviation of the uncertainty on the jet energy scale [20], and studying the corresponding variation of the MC signal yield. This quantifies in 2% for $t\bar{t}H$, and about 5% for the other production mechanisms. The larger jet multiplicity of the final state of $t\bar{t}H$ events contributes to minimizing the effect of this uncertainty.

Jet energy resolution: This uncertainty is evaluated by smearing the jet transverse momenta with the data/MC scale factors obtained in the jet resolution measurements, performed in γ+jet events. A somewhat worse (by about 10%) jet resolution is measured in data. This uncertainty is evaluated by comparing event yields with nominal and smeared simulated samples, and

corresponds to less than 1% for the $t\bar{t}H$ signal, and to about 1% for the other production mechanisms.

Lepton identification efficiency: For both electrons and muons, the uncertainty on the identification efficiency is computed varying the data/simulation scale factor by its uncertainty. The resulting difference in the signal efficiency estimated from the MC simulation is taken as systematic uncertainty (3% for electron, 1% for muons).

b-Tagging efficiency: This uncertainty is evaluated by modifying the measured b-tagging scale factors by one standard deviation of their uncertainty. The simulated signal yield changes by 1.3% in the leptonic channel and 1.1% in the hadronic channel.

$gg \rightarrow$ H contamination: This process contributes in part to the signal in the hadronic channel. The theoretical predictions are not reliable in this regime where the Higgs boson is produced in association to a multitude of jets $N_{jets} \geq 5$ radiated from the gluon-gluon initial state, the additional radiation being produced mostly via parton showering by PYTHIA. We estimate the systematic uncertainty to this contribution from several independent sources, and combine them in quadrature: the MC statistics for this sample is enhanced by mediating over several samples with different Higgs boson masses. We estimate the uncertainty on the production of a large number of jets in $gg \rightarrow H$ production as simulated by POWHEG, by taking the observed difference between POWHEG predictions and data in $t\bar{t}$ + jets events (which are dominated by gluon fusion production $gg \rightarrow t\bar{t}$) where the $t\bar{t}$ events decay leptonically [32]. This uncertainty is 30% in the bins with the largest discrepancy. We scale the fraction of $gg \rightarrow H$ plus heavy flavor jets by the observed difference in $t\bar{t}bb$ and $t\bar{t}qq$ events between data and POWHEG predictions [33], and take as uncertainty the data-MC discrepancy observed in data. Due to the small contamination of the $gg \rightarrow H$ background, the resulting large uncertainty on this process reflects into a small uncertainty on the total number of Higgs boson events.

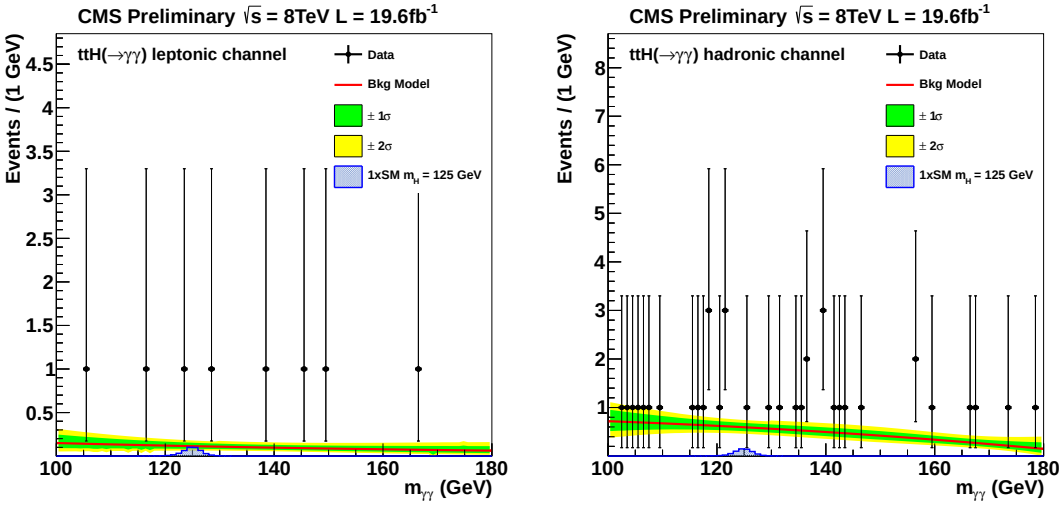

Figure 3: Diphoton invariant mass distribution for candidate $t\bar{t}H$ events passing the leptonic selection (left plot) and the hadronic selection (right plot).

6 Statistical Interpretation of the Results

No significant excess is observed in the mass spectra over the background expectations, hence we proceed computing an upper limit on the production cross section of a SM Higgs boson.

95% confidence level exclusion limits on the signal strength modifier are evaluated using a modified frequentist approach, CL_S, taking the profile likelihood ratio as a test statistic [34–36], similarly to Ref.[16].

The limits on the production cross section times branching ratio of a Higgs boson decaying to two photons relative to the SM expectation, are shown in Figure 4, for the leptonic (left) and hadronic (right) channels. The expected limit is shown as a dotted black line, and the bands corresponding to 68% (green) and 95% (yellow) probability are added. The observed limit is signalled by the black solid line. As can be seen the hadronic channel observes a limit of 6.8 times the SM cross section, compared to an expectation of 9.2 times the SM expectation. The upper limit observed in the leptonic channel corresponds to a cross section of 10.7 times the SM, compared to an expected limit of 8.0.

	Observed	Expected	Expected (No Syst.)
Hadronic Channel	6.8	9.2	8.8
Leptonic Channel	10.7	8.0	7.7
Combined	5.4	5.3	5.1

Table 2: Summary of observed and expected 95% upper limits to the production cross section of a standard model Higgs boson with mass $m_H = 125$ GeV : the observed, expected and expected limit neglecting systematic uncertainties are given for the hadronic channel, the leptonic channel, and their combination.

The two channels are combined, and the resulting upper limit is shown in Fig. 5. An upper limit of 5.4 times the SM cross section times branching ratio is observed at $m_H = 125$ GeV, compared to an expected limit of 5.3 times the SM predictions. The effect of the systematic uncertainties is limited with the current statistics, the expected limit being about 6% more stringent if systematics uncertainties are neglected. The observed and expected 95% upper limits are summarized in Table 2.

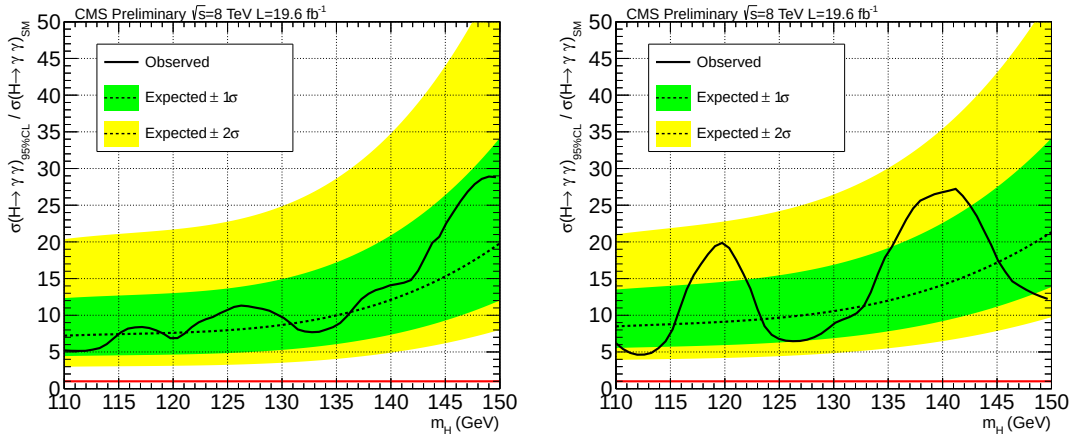

Figure 4: 95% C.L. upper limit on $t\bar{t}H$, $H \to \gamma\gamma$ production with leptonic (left) or hadronic (right) $t\bar{t}$ decays, divided by the SM production cross section times branching ratio.

In addition to setting limits on the $t\bar{t}H$ domimated Higgs boson production in this channels, one can also measure the signal strength μ_{ttH} defined as the ratio between the measured σ_{ttH} cross section and the expected standard model one, σ_{ttH}, $\mu_{ttH} = \sigma_{ttH}/\sigma_{ttH_{SM}}$. In doing so, it is assumed that the contribution of the additional Higgs boson production modes is exactly the one predicted by the SM. The measured signal strength is $\mu_{ttH} = -0.2^{+2.4}_{-1.9}$ for an assumed Higgs

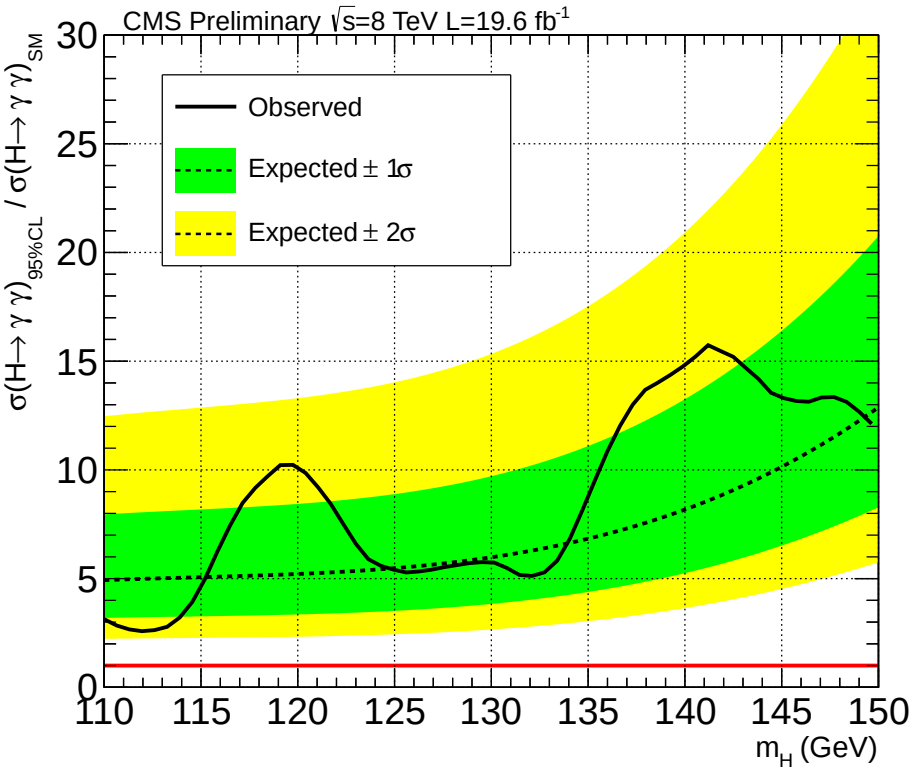

Figure 5: 95% C.L. upper limit on $t\bar{t}H$, $H \to \gamma\gamma$ production combining the results of the leptonic and hadronic channel, divided by the SM production cross section times branching ratio.

boson mass of 125.5 GeV. Figure 6 shows the likelihood as a function of μ_{ttH} for the combination of the leptonic and hadronic samples.

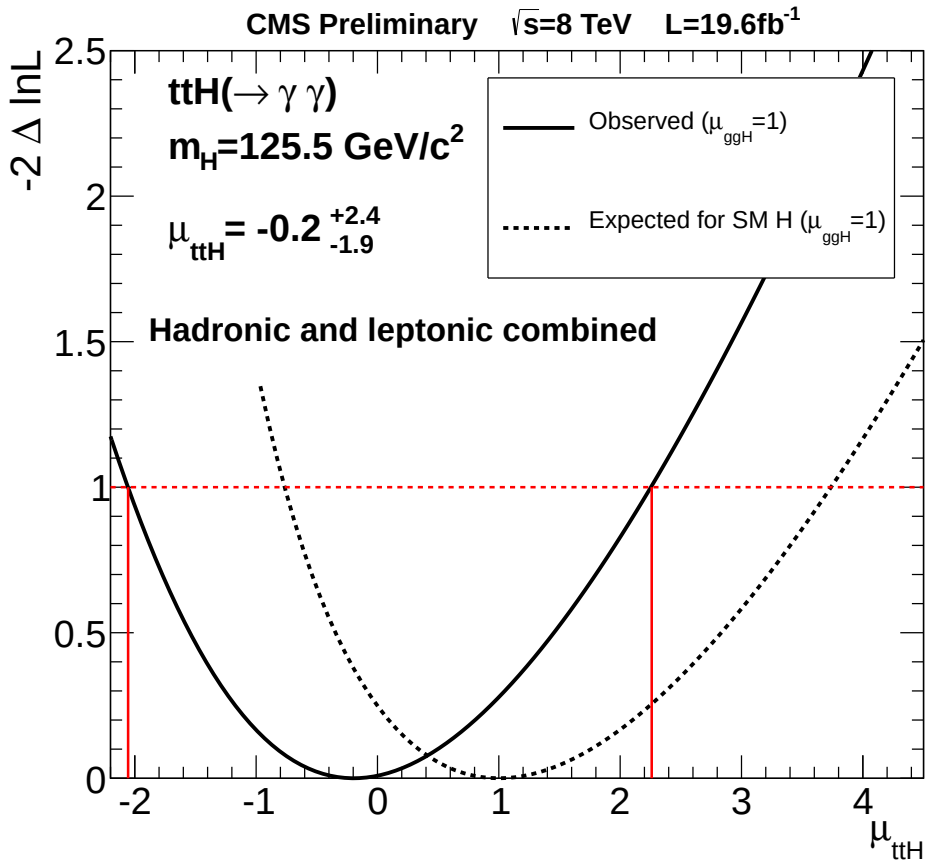

Figure 6: Likelihood of the combined signal strength $\mu_{ttH} = \sigma_{ttH}/\sigma_{ttH_{SM}}$ for the two categories, where $m_H = 125.5\,\text{GeV}$ and the signal strength for the other Higgs boson production mechanism is fixed to be 1. The solid line shows the observed signal strength while the dashed line shows the expected one. The red vertical lines define the 68% coverage region. The uncertainties include both statistical and systematic sources.

7 Conclusions

The first search for $t\bar{t}H$ production in events where the Higgs boson decays to two photons is presented. In order to maximize acceptance and sensitivity to such a small signal, we device two different sets of event selection criteria, optimized for leptonic and hadronic $t\bar{t}$ decays. An analysis of 19.6 fb^{-1} of 8 TeV pp collisions reveals no significant excess over background-only predictions, thus we proceed to set an observed (expected) 95% confidence level upper limit on the $t\bar{t}H$ production cross section times $BR(H \to \gamma\gamma)$ of 5.4 (5.3) times the standard model value, corresponding to 1.6 fb, for an assumed Higgs boson mass of 125 GeV.

References

[1] CMS Collaboration, "Observation of a new boson at a mass of 125 GeV with the CMS experiment at the LHC", *Phys. Lett. B* **716** (2012) 30, doi:10.1016/j.physletb.2012.08.021.

[2] ATLAS Collaboration, "Observation of a new particle in the search for the Standard Model Higgs boson with the ATLAS detector at the LHC", *Phys. Lett. B* **716** (2012) 1, doi:10.1016/j.physletb.2012.08.020.

[3] LHC Higgs Cross Section Working Group et al., "Handbook of LHC Higgs Cross Sections: 1. Inclusive Observables", *CERN-2011-002* (CERN, Geneva, 2011) arXiv:1101.0593.

[4] CMS Collaboration, "Top mass combination", CMS Physics Analysis Summary CMS-PAS-TOP-11-018, (2011).

[5] CDF and D0 Collaborations Collaboration, "Combination of the top-quark mass measurements from the Tevatron collider", *Phys. Rev. D* **86** (Nov, 2012) 092003, doi:10.1103/PhysRevD.86.092003.

[6] N. Arkani-Hamed, A. G. Cohen, and H. Georgi, "Electroweak symmetry breaking from dimensional deconstruction", *Phys. Lett. B* **513** (2001), no. 1-2, 232 – 240, doi:10.1016/S0370-2693(01)00741-9.

[7] N. Arkani-Hamed et al., "The Littlest Higgs", *JHEP* **02** (2002), no. 07, 034.

[8] R. Contino, L. Da Rold, and A. Pomarol, "Light custodians in natural composite Higgs models", *Phys. Rev. D* **75** (Mar, 2007) 055014, doi:10.1103/PhysRevD.75.055014.

[9] M. Carena et al., "Light Kaluza-Klein states in Randall-Sundrum models with custodial", *Nucl. Phys. B* **759** (2006), no. 1-2, 202 – 227, doi:10.1016/j.nuclphysb.2006.10.012.

[10] D∅ Collaboration, "Search for the Standard Model Higgs boson in the $t\bar{t}H \to t\bar{t}b\bar{b}$ channel", *D∅ Conference Note* **D0 CONF-5739** (2008).

[11] CDF Collaboration, "Search for the Standard Model Higgs Boson Produced in Association with Top Quarks Using the Full CDF Data Set", *Phys. Rev. Lett.* **109** (Nov, 2012) 181802, doi:10.1103/PhysRevLett.109.181802.

[12] ATLAS Collaboration, "Search for the Standard Model Higgs boson produced in association with top quarks in proton-proton collisions at $\sqrt{s} = 7$TeV using the ATLAS detector", *ATLAS Conference Report* **ATLAS-CONF-2012-135** (2012).

[13] CMS Collaboration, "Search for the standard model Higgs boson produced in association with a top-quark pair in pp collisions at the LHC", *CERN-PH-EP-2013-027* (2013) arXiv:1303.0763.

[14] A. Djouadi, J. Kalinowski, and M. Spira, "HDECAY: A Program for Higgs boson decays in the standard model and its supersymmetric extension", *Comput. Phys. Commun.* **108** (1998) 56–74, doi:10.1016/S0010-4655(97)00123-9, arXiv:hep-ph/9704448.

[15] CMS Collaboration, "Absolute Calibration of the Luminosity Measurement at CMS: Winter 2012 Update", CMS Physics Analysis Summary CMS-PAS-SMP-12-008, (2012).

[16] CMS Collaboration, "Updated measurements of the Higgs boson at 125 GeV in the two photon decay channel", *CMS Physics Analysis Summary* **CMS-PAS-HIG-13-001** (2013).

[17] CMS Collaboration, "The CMS experiment at the CERN LHC", *JINST* **3** (2008) S08004, doi:10.1088/1748-0221/3/08/S08004.

[18] CMS Collaboration, "Particle-Flow Event Reconstruction in CMS and Performance for Jets, Taus, and E_T^{miss}", CMS Physics Analysis Summary CMS-PAS-PFT-09-001, (2009).

[19] M. Cacciari, G. P. Salam, and G. Soyez, "The anti-k_t jet clustering algorithm", *JHEP* **04** (2008) 063, doi:10.1088/1126-6708/2008/04/063, arXiv:0802.1189.

[20] CMS Collaboration, "Determination of jet energy calibration and transverse momentum resolution in CMS", *JINST* **6** (2011) P11002, doi:10.1088/1748-0221/6/11/P11002, arXiv:1107.4277.

[21] M. Cacciari, G. P. Salam, and G. Soyez, "The catchment area of jets", *JHEP* **04** (2008) 005, doi:10.1088/1126-6708/2008/04/005, arXiv:0802.1188.

[22] CMS Collaboration, "Identification of b-quark jets with the CMS experiment", (2012). arXiv:1211.4462.

[23] CMS Collaboration, "Performance of CMS muon reconstruction in pp collision events at $\sqrt{s} = 7$ TeV", *JINST* **7** (2012) P10002, doi:10.1088/1748-0221/7/10/P10002, arXiv:1206.4071.

[24] CMS Collaboration, "Electron reconstruction and identification at $\sqrt{s} = 7$ TeV", CMS Physics Analysis Summary CMS-PAS-EGM-10-004, (2010).

[25] CMS Collaboration, "Measurements of inclusive W and Z cross sections in pp collisions at $\sqrt{s} = 7$ TeV", *JHEP* **01** (2011) 080, doi:10.1007/JHEP01(2011)080, arXiv:1012.2466.

[26] T. Sjöstrand, S. Mrenna, and P. Z. Skands, "PYTHIA 6.4 physics and manual", *JHEP* **05** (2006) 026, doi:10.1088/1126-6708/2006/05/026, arXiv:hep-ph/0603175.

[27] P. Nason, "A New method for combining NLO QCD with shower Monte Carlo algorithms", *JHEP* **11** (2004) 040, doi:10.1088/1126-6708/2004/11/040, arXiv:hep-ph/0409146.

[28] S. Frixione, P. Nason, and C. Oleari, "Matching NLO QCD computations with parton shower simulations: the POWHEG method", *JHEP* **11** (2007) 070, doi:10.1088/1126-6708/2007/11/070, arXiv:0709.2092.

[29] S. Alioli et al., "A general framework for implementing NLO calculations in shower Monte Carlo programs: the POWHEG BOX", *JHEP* **06** (2010) 043, doi:10.1007/JHEP06(2010)043, arXiv:1002.2581.

[30] R. Field, "Early LHC Underlying Event Data - Findings and Surprises", arXiv:1010.3558.

[31] GEANT4 Collaboration, "GEANT4—a simulation toolkit", *Nucl. Instrum. Meth. A* **506** (2003) 250, doi:10.1016/S0168-9002(03)01368-8.

[32] CMS Collaboration, "Measurement of Jet Multiplicity Distributions in Top Quark Events With Two Leptons in the Final State at a centre-of-mass energy of 7 TeV", *CMS Physics Analysis Summary* **CMS-PAS-TOP-12-023** (2012).

[33] CMS Collaboration, "First Measurement of the cross section ratio ttbb/ttjj in pp Collisions at $\sqrt{s} = 7$ TeV", *CMS Physics Analysis Summary* **CMS-PAS-TOP-12-024** (2012).

[34] A. Read, "Modified frequentist analysis of search results (the CL_s method)", Technical Report CERN-OPEN-2000-005, CERN, (2000).

[35] T. Junk, "Confidence level computation for combining searches with small statistics", *Nucl. Instrum. Meth. A* **434** (1999) 435, doi:10.1016/S0168-9002(99)00498-2, arXiv:hep-ex/9902006.

[36] ATLAS and CMS Collaborations, LHC Higgs Combination Group, "Procedure for the LHC Higgs boson search combination in Summer 2011", ATL-PHYS-PUB/CMS NOTE 2011-11, 2011/005, (2011).